Spatial Sensor Layout Optimization for Radio Environment Map Construction

Qianhao Gao[1], Qiuming Zhu[1], Zhipeng Lin[1], Yi Zhao[1], Jie Wang[1], Weizhi Zhong[2], Yang Huang[1], Qihui Wu[1]
[1]*The College of Electronic and Information Engineering, Nanjing University of Aeronautics and Astronautics, Nanjing, China.*
[2]*The College of Astronautics, Nanjing University of Aeronautics and Astronautics, Nanjing, China.*
Email:{qianhaogao, zhuqiuming, linlzp, zhaoyi, bx2104906wangjie, zhongwz, yang.huang.ceie}@nuaa.edu.cn, wuqihui2014@sina.com

***Abstract*—Radio environment map (REM) can visually display the spectrum situation and play a significant role in spectrum monitoring and management. In this paper, an efficient layout optimization of spectrum sensors for REM construction is proposed, which involves the minimum number of sampling sensors and an optimal layout. Firstly, the semi-variogram function, rather than the correlation function, is adopted to derive the correlation distance (or the spatial sampling interval), and then the minimum required number of sensors is determined. Secondly, we propose a Local linear approximation-Voronoi (L-Voronoi)-based sampled position scoring criteria as well as the spatial covariance-based uncertainty metric. By evaluating the effectiveness of sampled positions and the uncertainty of unsampled positions, the positions of sensors are adjusted online. Finally, the proposed layout scheme is verified and evaluated by the simulated REM data. Numerical results demonstrate that its construction error is 4.26%-41.18% better than those of traditional layout methods.**

***Index Terms*—Radio environment map, spatial sampling, propagation model, spectrum cartography, sensor optimization.**

I. Introduction

With the increasement of electronic devices such as radios, radars and navigation systems, the electromagnetic environment has become increasingly complex [1]–[3]. The radio environment map (REM), also known as the spectrum environment map (SEM), enables the visualization of spectrum information including time, frequency, received signal strength (RSS), and RF emitter positions, on a geographical map [4]–[6]. It is useful in monitoring, management, and security of spectrum resources [7]–[9].

The key process of spectrum cartography is to recover the data of unsampled positions based on the measured data via distributed sensors [10], [11]. When the number of sensors is limited, it becomes challenging to arrange the distributed sensors in order to guarantee the best recovery accuracy. Note that it can be viewed as a spatial sampling problem, which is a hot topic in the geoscience field [12]. Several statistical mathematics tools have been developed to explore the spatial sampling. However, these schemes aim to obtain the statistical features in the region of interest (ROI) rather than recover the data of unknown positions.

The existing sensor layout schemes can be mainly divided into two categories, batch layout and online layout [12]–[20]. The former refers to deploying all the sensors at once. It's more suitable for the initial planning or static spectrum environment. In [14], the authors compared two methods, i.e., square lattice layout and randomly layout. The experiments shown that the random layout is more suitable for the location of RF emitters. Some researchers studied the layout optimizations based on the REM construction accuracy. For example, compressed sensing is a widely used construction method and the authors in [15] adjusted the sampling positions by optimizing the sensing matrix. In [16], the authors optimized the layout by reducing the column correlation in a more efficient way. The authors in [17] established a more complex REM model and developed a spatial sampling matrix optimization algorithm. It was based on the maximum mutual information criterion and could improve the recovery accuracy. However, the batch sampling schemes do not consider the local features and cannot dynamically update the sampling positions.

Some sequential sampling schemes, or online optimization algorithms, can be addressed recently in [18]–[20]. Based on the uncertainty metric of posterior variance, the authors in [18] proposed a sampling scheme for unmanned aerial vehicle (UAV)-aided spectrum cartography. It was assumed that the region with larger posterior variance was more informative. By constructing a residual neural network, they further proposed a Convolutional Neural Network (CNN)-based uncertainty metric [19]. Note that the online sampling method is highly susceptible to fall into local optima. The authors in [20] employed a state-of-art adaptive mesh strategy Local linear approximation-Voronoi (L-Voronoi) to conduct spectrum data collection in indoor scenarios. However, this method is not applicable to spectrum cartography, as it only offers a scoring mechanism for the sampled points and lacks a systematic approach for

This work was supported in part by the National Natural Science Foundation of China under Grants No. 62271250, No. U23B2005 and No. 62401260, in part by the Natural Science Foundation of Jiangsu Province under Grants No. BK20211182 and No. SBK2024047654, in part by the Key Technologies R&D Program of Jiangsu (Prospective and Key Technologies for Industry) under Grants No. BE2022067, No. BE2022067-3, and No. BE2022067-1, in part by States Key Laboratory of Air Traffic Management System under Grant No. SKLATM202305, and in part by Shanghai Aerospace Science and Technology Fund under Grant No. SAST2023-023.

selecting the next sampling point.

To fill these research gaps, an efficient layout scheme for REM construction is proposed in this paper. The main novelties and contributions are summarized as follows.

1) A sensor layout scheme for REM construction with limited sensors is proposed. Based on the derived spatial correlation distance, the minimum number of sensors is determined and the corresponding layout is optimized online.

2) The minimum sensor number is analyzed based on the random field theory. By introducing the spatial correlation distance and semi-variogram function, the theoretical expression of minimum number of sensors is derived.

3) A hybrid optimization method combining backward sampling and forward sampling is proposed. The L-Voronoi score is employed as a measure of redundancy to remove old sensors and the spatial covariance is used as an uncertainty measure to add new sensors.

II. Proposed Sensor Layout Scheme

The region of interest (ROI) with the spatial dimension of $W_x \times W_y$ is firstly discretized into small grids. It can be described by a spectrum $\mathbf{C} \in \Re^{N_x \times N_y}$, where N_x and N_y indicate the grid number along x and y dimensions, respectively. Each element or grid is colored according to its RSS value. The sensors are arranged in the center of the grid to obtain the RSS value of the entire grid. Technically, REM reconstruction aims to recovery all RSS values, i.e., $N = N_x \times N_y$ grids, based on the known values at the sampled grids.

The positions of all grids are demoted as $\{\mathbf{p}_n \in \mathbf{P} | n = 1, 2, ..., N\}$, where $\mathbf{p}_n = (x_n^p, y_n^p)$. Suppose that we select M from N grids, denoted by $\left\{\tilde{\mathbf{p}}_m \in \tilde{\mathbf{P}} | m = 1, 2, ..., M\right\}$, where $\tilde{\mathbf{p}}_m = \left(x_m^{\tilde{p}}, y_m^{\tilde{p}}\right)$ is the location of m-th sensor. The sampled data set via deployed sensors is defined as

$$\tilde{\mathbf{C}} = S_{\tilde{\mathbf{P}}}(\mathbf{C}) = \begin{cases} c(\mathbf{p}), \mathbf{p} \in \tilde{\mathbf{P}}, \\ 0, \text{else}. \end{cases} \tag{1}$$

where $S_{\tilde{\mathbf{P}}}(\cdot)$ is the sampling operator.

The construction problem is to estimate the REM matrix $\hat{\mathbf{C}}$ based on $\tilde{\mathbf{C}}$. It can be modeled to minimize the difference between $\hat{\mathbf{C}}$ and $\mathbf{C}$ as

$$\begin{aligned} &\min_{\hat{\mathbf{C}}} ||\hat{\mathbf{C}} - \mathbf{C}||_F^2, \\ &\text{s.t. } \hat{c}(\mathbf{p}) = c(\mathbf{p}), \mathbf{p} \in \tilde{\mathbf{P}}, \end{aligned} \tag{2}$$

where $|| \cdot ||_F^2$ denotes the Frobenius norm, which means the square root of the sum of absolute square of matrixs elements.

Firstly, we randomly place the minimum number of sensors to obtain an initial situation. The sensor is then adjusted one by one to achieve best construction accuracy. The flowchart of proposed optimization process is shown in Fig. 1. The nonlinear Voronoi score is calculated to evaluate the redundancy of each sensor and then eliminate the one with worst redundancy. Meanwhile, the spatial covariance is evaluated to quantify the uncertainty at unsampled positions in order to determine the position that the removed sensor can be moved to. Finally,

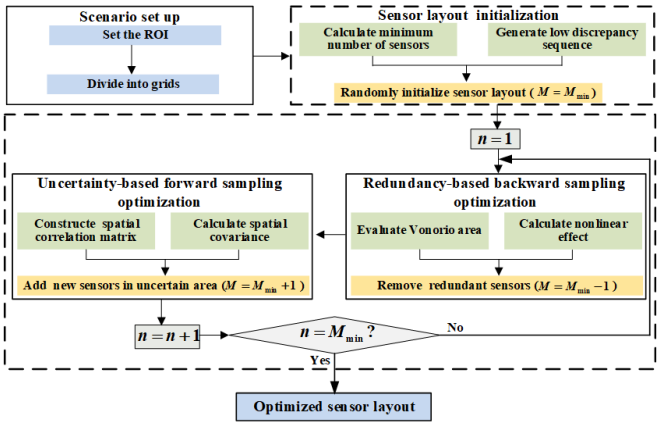

Fig. 1. The flowchart of proposed layout optimization.

by the iterations of above two steps, all sensors' position can be optimized.

III. Optimization of Sensor Number and Positions

A. Minimum number of sensors

For an arbitrary grid $\mathbf{p}_n$, $C(\mathbf{p}_n) = C(x_n^p, y_n^p)$ is referred as the corresponding random field. For simplify, we denote the position of grid as z_p. The average field within the distance of h can be derived as

$$C_h(z_p) = \frac{1}{h} \int_{z_p - \frac{h}{2}}^{z_p + \frac{h}{2}} C(z_p) \mathrm{d}z_p, \tag{3}$$

where h is the average spatial distance.

The variance reduction function can be expressed as

$$\Gamma_C^2(h) = \frac{\mathrm{Var}[\mathrm{C}_h(z_p)]}{{\sigma_C}^2} = \frac{2}{h} \int_0^h (1 - \frac{\tau}{h}) \rho_C(\tau) \mathrm{d}\tau, \tag{4}$$

where σ_C^2 is the variance of the random field, $\rho_C(\tau)$ is the correlation function, and $\mathrm{Var}[\cdot]$ is the variance operator. Then, the scale of fluctuation (or correlation distance) δ_d, can be defined as

$$\delta_d = \lim_{h \to \infty} h \Gamma_C^2(h) = 2 \int_0^{+\infty} \rho_C(\tau) \mathrm{d}\tau. \tag{5}$$

In this paper, we use semi-variogram function $\gamma_C(\tau)$ rather than correlation function $\rho_C(\tau)$ to calculate the correlation distance. The relationship is

$$\rho_C(\tau) = sill_C - \gamma_C(\tau), \tag{6}$$

where $sill_C = \sigma_C^2 + \varepsilon_C$, and ε_C is caused by measurement error, which reflects the spatial small-scale variability.

The correlation distance δ_d can be expressed as

$$\delta_d = 2 \int_0^{+\infty} sill_C - \gamma_C(\tau) \mathrm{d}\tau. \tag{7}$$

Note that, the term in the semi-variogram function can offset $sill_C$, which ensures the finite of integration. Thus, the correlation distance is a constant value. Finally, combining

the Nyquist sampling law, the minimum number of sensors can be estimated as

$$M_{min} = \frac{4 * W_x * W_y}{\delta_d^2}. \tag{8}$$

where W_x and W_y are the length and width of ROI.

B. Redundancy-based backward sampling

The initial sensor layout is not optimal due to lack of real data. It is necessary to remove some redundant sensors for the enhancement of sensor utilization after obtaining some data. In this paper, based on the global uniformity and local nonlinearity, we introduce the redundancy measure to evaluate the importance of each sensor. Redundancy can be defined by two factors as

$$Q(\tilde{\mathbf{p}}_m) = \frac{\mu \cdot V(\tilde{\mathbf{p}}_m)}{\sum_{m=1}^{M} V(\tilde{\mathbf{p}}_m)} + \frac{(1-\mu) \cdot G(\tilde{\mathbf{p}}_m)}{\sum_{m=1}^{M} G(\tilde{\mathbf{p}}_m)}, \tag{9}$$

where $V(\tilde{\mathbf{p}}_m)$ is the uniformity throughout the entire region, $G(\tilde{\mathbf{p}}_m)$ is the nonlinearity in the local region, and μ is the weight parameter. Specifically, the global uniformity can be defined as the size of Voronoi cell. Each Voronoi cell contains only one sensor, and the cell size can be defined as

$$V(\tilde{\mathbf{p}}_m) = k_m, \tag{10}$$

where k_m denotes the number of experimental points $\mathbf{t}_k$ closest to node $\tilde{\mathbf{p}}_m$,

$$\begin{gathered} k_m = ||\mathbf{e}_m||_0, \\ \{\mathbf{e}_m \in \mathbf{E}, ||\mathbf{e}_m - \tilde{\mathbf{p}}_m||_2 \leq ||\mathbf{e}_m - \tilde{\mathbf{p}}_{m'}||_2, m \neq m'\}, \end{gathered} \tag{11}$$

where $|||\mathbf{e}_m||_0$ is the number of point set $\mathbf{e}_m$ and $\mathbf{E}$ is the set of the experimental point.

Moreover, the nonlinearity is estimated by the gradient $\nabla[c(\tilde{\mathbf{p}}_m)]$, which can be calculated by the least squares estimation for the sensor $\tilde{\mathbf{p}}_m$ and its neighbor sensors $\tilde{\mathbf{p}}_{m1}, \tilde{\mathbf{p}}_{m2}, ..., \tilde{\mathbf{p}}_{mb}$ as

$$\nabla[c(\tilde{\mathbf{p}}_m)] = \begin{bmatrix} \tilde{\mathbf{p}}_{m1}^x - \tilde{\mathbf{p}}_m^x & \tilde{\mathbf{p}}_{m1}^y - \tilde{\mathbf{p}}_m^y \\ \tilde{\mathbf{p}}_{m2}^x - \tilde{\mathbf{p}}_m^x & \tilde{\mathbf{p}}_{m2}^y - \tilde{\mathbf{p}}_m^y \\ \cdots & \cdots \\ \tilde{\mathbf{p}}_{mb}^x - \tilde{\mathbf{p}}_m^x & \tilde{\mathbf{p}}_{mb}^y - \tilde{\mathbf{p}}_m^y \end{bmatrix}^{-1} \begin{bmatrix} c(\tilde{\mathbf{p}}_{m1}) \\ c(\tilde{\mathbf{p}}_{m2}) \\ \cdots \\ c(\tilde{\mathbf{p}}_{mb}) \end{bmatrix}, \tag{12}$$

where $c(\tilde{\mathbf{p}}_{m1})$ is the RSS value. Then, through Taylor series expansion, the local nonlinearity is obtained by differences between the RSS of the neighbors and the local linear approximation as

$$G(\tilde{\mathbf{p}}_m) = \sum_{i=1}^{b} |c(\tilde{\mathbf{p}}_{mi}) - (c(\tilde{\mathbf{p}}_m) + \nabla[c(\tilde{\mathbf{p}}_m)](\tilde{\mathbf{p}}_{mi} - \tilde{\mathbf{p}}_m))|, \tag{13}$$

where b is the number of neighbor sensors.

Then, the sensor with lowest redundancy can be found by using a brute-force search to solve the following problem as

$$\begin{aligned} &\mathbf{p}_{remove} = \arg\min_{\mathbf{p}} Q(\tilde{\mathbf{p}}_m), \\ &\text{s.t. } \tilde{\mathbf{p}}_m \in \tilde{\mathbf{P}}, m = 1, 2, ..., M, \end{aligned} \tag{14}$$

Thus, all redundant sensors can be removed one by one.

C. Uncertainty-based forward sampling

To arrange a new sensor, we introduce an uncertainty measurement based on the spatial covariance to assess the importance of unknown region, and the put it at the place with greater importance.

Spatial covariance represents the spatial variability between two positions. It can reflect the difference between the unknown and known positions based on the information of deployed sensors. The greater difference indicates the greater value changing [21]. Thus, we define the uncertainty as

$$U(\mathbf{p}_l) = \sum_{i=1}^{M} \lambda_i \cdot \gamma(||\tilde{\mathbf{p}}_i - \mathbf{p}_l||_2) - \phi, \tag{15}$$

where λ_i is the weight coefficients, and $\gamma(||\tilde{\mathbf{p}}_i - \mathbf{p}_l||_2)$ is the semi-variance between sampled positions $\left\{\tilde{\mathbf{p}}_m \in \tilde{\mathbf{P}} | m = 1, 2, ..., M\right\}$ and unsampled positions $\{\mathbf{p}_l \in \mathbf{P} - \tilde{\mathbf{P}} | l = 1, 2, ..., L\}$.

The semi-variance can be obtained by the mean RSS estimation of grid $\mathbf{p}_l$ via a minimum mean square error (MMSE) estimator. The weight coefficient can be calculated by

$$\begin{bmatrix} \gamma(||\tilde{\mathbf{p}}_1 - \tilde{\mathbf{p}}_1||_2) & \gamma(||\tilde{\mathbf{p}}_1 - \tilde{\mathbf{p}}_2||_2) & \cdots & \gamma(||\tilde{\mathbf{p}}_1 - \tilde{\mathbf{p}}_M||_2) & 1 \\ \gamma(||\tilde{\mathbf{p}}_2 - \tilde{\mathbf{p}}_1||_2) & \gamma(||\tilde{\mathbf{p}}_2 - \tilde{\mathbf{p}}_2||_2) & \cdots & \gamma(||\tilde{\mathbf{p}}_2 - \tilde{\mathbf{p}}_M||_2) & 1 \\ \cdots & \cdots & \cdots & \cdots & \cdots \\ \gamma(||\tilde{\mathbf{p}}_M - \tilde{\mathbf{p}}_1||_2) & \gamma(||\tilde{\mathbf{p}}_M - \tilde{\mathbf{p}}_2||_2) & \cdots & \gamma(||\tilde{\mathbf{p}}_M - \tilde{\mathbf{p}}_M||_2) & 1 \\ 1 & 1 & 1 & 1 & 0 \end{bmatrix} \begin{bmatrix} \lambda_1 \\ \lambda_2 \\ \cdots \\ \lambda_M \\ -\phi \end{bmatrix} = \begin{bmatrix} \gamma(||\tilde{\mathbf{p}}_1 - \mathbf{p}_l||_2) \\ \gamma(||\tilde{\mathbf{p}}_2 - \mathbf{p}_l||_2) \\ \cdots \\ \gamma(||\tilde{\mathbf{p}}_M - \mathbf{p}_l||_2) \\ 1 \end{bmatrix}. \tag{16}$$

Then, the position with the highest uncertainty among all unknown positions can be found by

$$\begin{aligned} &\mathbf{p}_{next} = \arg\max_{\mathbf{p}} U(\mathbf{p}_l), \\ &\text{s.t. } \mathbf{p}_l \in \mathbf{P} - \tilde{\mathbf{P}}, l = 1, 2, ..., L. \end{aligned} \tag{17}$$

Here, we can use Lagrangian method to solve (17) and deploy the next sensor accordingly. Thus, all sensors can be deployed in new locations by the above procedure.

IV. Simulation Results and Comparisons

In this section, the proposed scheme is verified by simulated REM data in a campus scenario. The scenario is about 1 km $\times$ 1 km. It mainly includes buildings, roads, forests, and lakes. The height of buildings is between 19 and 55 meters. We simulate several different RF emitters, such as RF emitters carried by pedestrians, vehicle-mounted RF transmitters, and base stations. For simplicity, the transmitting power is set as 20 dBm and the center frequency is 2450 MHz. The rest parameters are shown in Table I. Ray tracing (RT) technology is a practical tool to predict the radio propagation and can be used to calculate the ideal REM data in the complex scenario [22]. The satellite

TABLE I
SIMULATION PARAMETERS

Parameter	Value			
	Index	Height (m)	Power(dBm)	Antenna type
RF emitter setting	1	1.5	20	Isotropic
	2	1.5	20	Isotropic
	3	1.5	20	Isotropic
	4	1	20	Isotropic
	5	1	20	Isotropic
	6	20	20	Directional
	7	30	20	Isotropic
	8	2	20	Isotropic
Center frequency	2.45 GHz			
Bandwidth	10 MHz			
Cartography area	1 km × 1 km			
Grid resolution	10 m × 10 m			

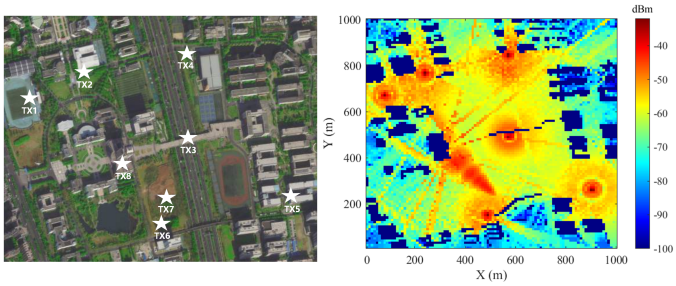

Fig. 2. The satellite view of campus scenario and RT-based ideal REM.

view of scenario and the RT-based REM data are shown in Fig. 2.

Based on the simulated data, we can calculate the spatial correlation and obtain the experimental semi-variances. Then, we fit the experimental semi-variance using Gaussian, spherical, and exponential models, as shown in Fig. 3. The experimental semivariance demonstrates that an upward trend before reaching 250 m, followed by a fluctuation beyond that range. The correlation distances obtained from these three models are 226.56 m, 217.98 m, and 226.883 m, respectively. The initial number of sensors is around 81.

To validate the effectiveness, we compare the REM construction performance with 5% sampled data by four layout schemes, i.e., random layout, regular layout, spatial sampling points (SSP) layout [16], and the proposed one. Note that the other three schemes are batch layout schemes. For the proposed online scheme, we randomly place the initial sensors and adjust all sensors one by one. The layout results of four schemes are shown in Fig. 4. Random layout and SSP layout lead to more sensors next to each other, which is actually not conducive to efficient data acquisition. While regular layout and the proposed layout can reduce the phenomenon. By locally amplifying two typical areas (the area with drastic RSS changes and the area with slow RSS changes), it can be observed that the proposed layout places more sensors in critical areas to improve construction accuracy and fewer sensors in less crucial areas to reduce redundancy, compared to other schemes.

The constructed REMs by different layout schemes are shown in Fig. 5, where the inverse distance weighting method is used to recover the data at the unsampled positions. It can

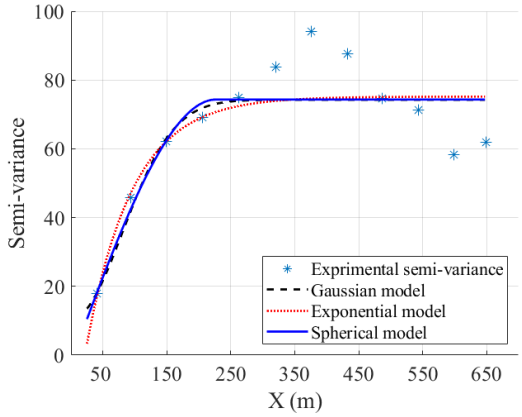

Fig. 3. Semi-variance and spatial correlation distance.

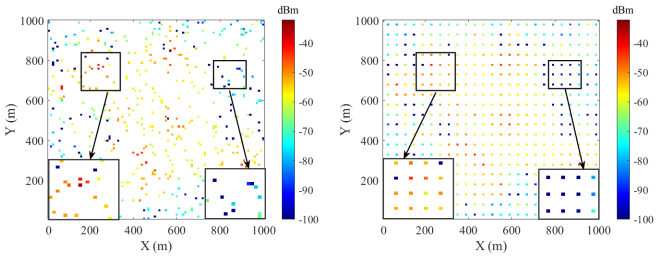

(a) Random layout (b) Regular layout

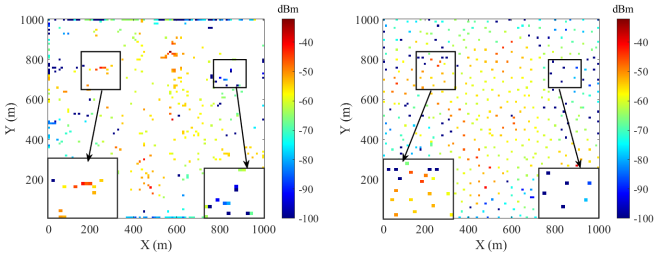

(c) SSP layout (d) Proposed layout

Fig. 4. Sensor layouts of different schemes

be seen that the deep blue regions have very low RSS values due to the blockage of buildings. Comparing with the ideal REM, the proposed scheme outperforms others. For further quantitative comparison purpose, we define the mean absolute error (MAE) as the average difference between recovered and ideal RSS values at all girds. Fig. 6 compares the MAEs under the sampling percentage from 5% to 70%. It shows that as the sampling percentage increases, the MAEs of all methods decrease significantly. The proposed scheme outperforms other layout schemes by 0.4 to 0.7 dBm, which could up to 4.26% (Sampling rate 5%, 9.49) to 41.18% (Sampling rate 70%, 1.71) in the term of MAE.

V. CONCLUSIONS

In this paper, we have proposed an efficient sensor layout scheme for REM construction and spectrum cartography. We have incorporated the spatial random field theory to explore the

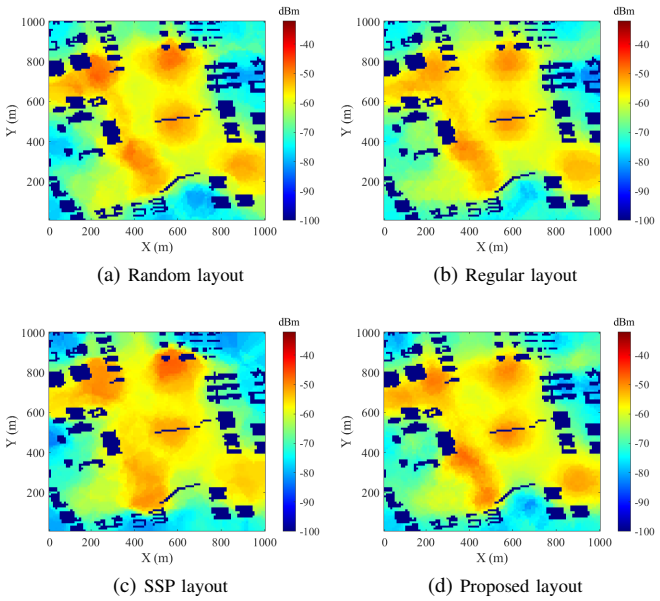

(a) Random layout (b) Regular layout

(c) SSP layout (d) Proposed layout

Fig. 5. REM reconstruction by different layout schemes

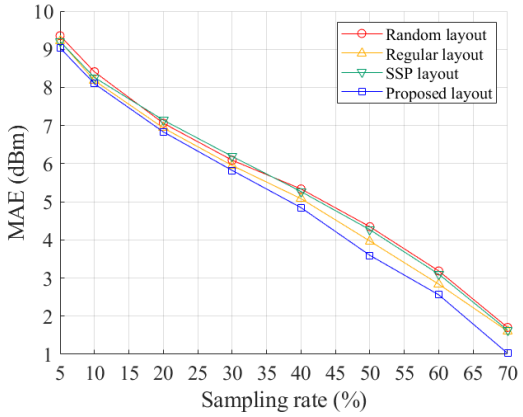

Fig. 6. MAEs of reconstructed REMs by different layout schemes.

spatial sampling interval and minimum number of sampling sensors. By utilizing the uncertainty metric for unknown positions and the scoring criteria for the sampled positions, we have sequentially optimized the sensor position. Simulation results have shown that the proposed scheme can achieve a better spatial coverage and improve the REM construction accuracy. Future research will involve extensive field tests to further optimize the layout scheme using measured data, and promote its application in 3D REM layout optimization.

REFERENCES

[1] Y. Zhao, Q. Zhu, Z. Lin, L. Guo, Q. Wu, J. Wang and W. Zhong, "Temporal prediction for spectrum environment maps with moving radiation sources," *IET Communications.*, vol. 17, no. 5, pp. 538-548, 2023.

[2] M. Shi, K. Yang, D. Niyato, H. Yuan, H. Zhou and Z. Xu, "The meta distribution of SINR in UAV-assisted cellular networks," *IEEE Transactions on Communications.*, vol. 71, no. 2, pp. 1193-1206, 2023.

[3] X. Zhao, F. Du, S. Geng, Z. Fu, Z. Wang, Y. Zhang, Z. Zhou, L. Zhang and L. Yang, "Playback of 5G and beyond measured MIMO channels by an ANN-based modeling and simulation framework," *IEEE Journal on Selected Areas in Communications.*, vol. 38, no. 9, pp. 1945-1954, 2020.

[4] W. Liu and J. Chen, "UAV-aided radio map construction exploiting environment semantics," *IEEE Transactions on Wireless Communications.*, vol. 22, no. 9, pp. 6341–6355, 2023.

[5] K. Mao, Q. Zhu, Y. Qiu, et al., "A UAV-aided real-time channel sounder for highly dynamic nonstationary A2G scenarios," *IEEE Transactions on Instrumentation and Measurement.*, vol. 72, pp. 1-15, 2023.

[6] A. Ahmad, S. Ahmad, M. H. Rehmani and N. U. Hassan, "A survey on radio resource allocation in cognitive radio sensor networks," *IEEE Communications Surveys and Tutorials.*, vol. 17, no. 2, pp. 888–917, Secondquarter. 2015.

[7] J. Pan, N. Ye, H. Yu, et al., "AI-driven blind signature classification for IoT connectivity: A deep learning approach," *IEEE Transactions on Wireless Communications.*, vol. 21, no. 8, pp. 6033-6047, 2022.

[8] C. He, Y. Dong and Z. J. Wang, "Radio map assisted multi-UAV target searching," *IEEE Transactions on Wireless Communications.*, vol. 22, no. 7, pp. 4698–4711, 2023.

[9] Y. Huang, H. Cui, Y. Hou, C. Hao, W. Wang, Q. Zhu, J. Li, Q. Wu and J. Wang, "Space-based electromagnetic spectrum sensing and situation awareness," *Space: Science & Technology.*, vol. 4, p. 0109, 2024.

[10] Q. Zhu, Y. Zhao, Y. Huang, Z. Lin, L. H. Wang, Y. Bai, T. Lan, F. Zhou and Q. Wu, "DEMO abstract: An UAV-based 3D spectrum real-time mapping system," *IEEE INFOCOM 2022 - IEEE Conference on Computer Communications Workshops (INFOCOM WKSHPS).*, New York, NY, USA, 2022, pp. 1-2.

[11] J. Wang, Q. Zhu, Z. Lin, J. Chen, G. Ding, Q. Wu, G. Gu and Q. Gao, "Sparse bayesian learning-based hierarchical construction for 3D radio environment maps incorporating channel shadowing," *IEEE Transactions on Wireless Communications.*, early access, 2024, doi: 10.1109/TWC.2024.3416447.

[12] D. J. Brus, "Statistical approaches for spatial sample survey: Persistent misconceptions and new developments," *European Journal of Soil Science.*, vol. 72, no. 2, pp. 686–703, 2021.

[13] J. Liu, J. Yu, D. Niyato, R. Zhang, X. Gao and J. An, "Covert ambient backscatter communications with multi-antenna tag," *IEEE Transactions on Wireless Communications.*, vol.22, no.9, pp.6199-6212, 2023.

[14] Y. -Q. Xu, B. Zhang, G. Ding, B. Zhao, S. Li and D. Guo, "Radio environment map construction based on spatial statistics and bayesian hierarchical model," *IEEE Transactions on Cognitive Communications and Networking.*, vol. 7, no. 3, pp. 767–779, 2021.

[15] K. Manohar, B. W. Brunton, J. N. Kutz and S. L. Brunton, "Data-driven sparse sensor placement for reconstruction: Demonstrating the benefits of exploiting known patterns," *IEEE Control Systems Magazine.*, vol. 38, no. 3, pp. 63–86, 2018.

[16] L. Wei, X. Mo, S. Sun and L. Gui, "Spatial sampling points selection for 3D REM construciton,"*2022 IEEE 8th International Conference on Computer and Communications (ICCC).*, Chengdu, China, 2022, pp. 2123–2127.

[17] J. Wang, Q. Zhu, Z. Lin, Q. Wu, et al. "Sparse bayesian learning-based 3D radio environment map construction—sampling optimization, scenario-dependent dictionary construction and sparse recovery," *IEEE Transactions on Cognitive Communications and Networking.*, vol.10, no.1, pp.80-93, 2024.

[18] D. Romero, R. Shrestha, Y. Teganya and S. P. Chepuri, "Aerial spectrum surveying: Radio map estimation with autonomous UAVs," *2020 IEEE 30th International Workshop on Machine Learning for Signal Processing (MLSP).*, Espoo, Finland, 2020. pp. 1–6.

[19] R. Shrestha, D. Romero and S. P. Chepuri, "Spectrum surveying: Active radio map sstimation with autonomous UAVs," *IEEE Transactions on Wireless Communications.*, vol. 22, no. 1, pp. 627–641, 2023.

[20] J. Yao, W. Tang, B. Li, S. Zhang and R. Sun, "Efficient indoor signal propagation model based on LOLA-Voronoi adaptive meshing," *Applied Computational Electromagnetic Society.*, vol. 34, no. 4, pp. 437–442, 2020.

[21] E. M. Schliep, K. Christopher and D. Ranadeep, "Correcting for informative sampling in spatial covariance estimation and kriging predictions," *Journal of Geographical Systems.*, pp. 1–27, 2023.

[22] K. Mao, Q. Zhu, C.-X. Wang, et al., "A survey on channel sounding technologies and measurements for UAV-assisted communications," *IEEE Transactions on Instrumentation and Measurement.*, Vol. 73, pp. 1–24, 2024.